npj | 2D Materials and Applications

www.nature.com/npj2dmaterials

REVIEW ARTICLE OPEN

Check for updates

# Electrical transport properties in group-V elemental ultrathin 2D layers

Zehan Wu[1,2] and Jianhua Hao[1,2]✉

After the breakthrough of the study on the two-dimensional (2D) layered phosphorus, group-V elemental ultrathin 2D layers have captured considerable attentions in recent years on account of their unique and promising electrical transport properties, including semiconductor features with direct and desirable energy band structures, outstanding carrier mobilities, controllable and tunable characteristics under applied strain, electric and magnetic fields, highly anisotropic phenomena along both in-plane and out-plane directions, topological transmission states, and negative Poisson's ratio. Accordingly, a number of investigations on this family of 2D materials have been conducting rapidly, while initiating great potential and new opportunities on the nanoscale science and applications in optoelectronic, magneto-electronics, thermo-electronic, ferroelectric, topological spintronics, and so on. Herein, a specific review is provided with systematical summarizations and refinements on the recent advances of the electrical transport in group-V elemental ultrathin 2D layers from the blossoming field of research, while comprehensive discussion and some recommendations are put forward, with an expectation of broadening and deepening understanding of the family of 2D layers. Lastly, we provide critical motivation and challenge for future explorations in this promising territory.

*npj 2D Materials and Applications* (2020)4:4 ; https://doi.org/10.1038/s41699-020-0139-x

## INTRODUCTION

Since the astonishing discovery of graphene (Gr)[1], the family of two-dimensional (2D) materials with layered structure had recently been emerged and developed by leaps and bounds, which opens a new door for further exploring various physical mechanisms that stemmed from quantum constraint or size effects in electronic and optical devices[2–8]. Numerous investigations have been reported on both theoretical and experimental frontiers about many classes of 2D materials, including elemental substances[9,10], transition metal dichalcogenides (TMDs)[11–14], group-III–VI compounds[15–17], metal carbides and nitrides (MXenes)[18,19], and so on. Among them, one class of elemental layers, derived from group-V materials (phosphorus, arsenic, antimony, and bismuth), has increasingly been attracted by researchers due to its profound development potential and broad prospect in electronic applications, as shown in Fig. 1. Particularly, differing from other layered elemental materials, these four group-V materials are fundamentally p-type semiconductors with tunable bandgaps in a broad range[20–22], which are found to exhibit relationship with layer number, temperature, or applied stain. These intriguing characteristics may offer new opportunities to develop ultrathin novel electronic devices at nanoscale. As such, it becomes increasingly important and imperative to give a summary and outlook on this research field, in order to satisfy the growing demand on the knowledge, especially electrical transport properties of group-V elemental 2D materials.

The attraction of group-V elemental ultrathin 2D layers began with the exploration of black phosphorene (BP). Few-layer BP has brought a great impact on the research of 2D materials because of its coexistence of direct bandgap and high carrier mobility[20,23–27]. A tunable bandgap of BP from ~0.3 eV for bulk to larger than 2 eV for monolayer was predicted and further confirmed, while a high hole mobility up to a few thousands $cm^2V^{-1}s^{-1}$ is able to be obtained in few-layer BP. Additionally, many other valuable properties are found and studied by measuring the electrical performance of phosphorene, including promising photoelectronic and thermo-electric characteristics, highly anisotropic and strain tunable properties in carrier transport, and 2D topological nature modulated by vertical electric field in specific devices[27–39]. These rich and specific electrical transport features make phosphorene promising for numerous electronic applications in the future, which has recently become a hot topic in 2D research field.

Although phosphorene shows enormous potential in electronic devices, one great challenge limiting further investigation of phosphorene is its comparatively unstable in ambient environment[40]. Alternatively, the researchers' eyes turned to other homologous group of phosphorus, including arsenic, antimony, and bismuth, which also possess layered structure in some of their naturally existed allotropes[41]. The promising features of monolayer arsenene, antimonene, and bismuthene, including appropriate energy bandgap, relative stability in natural environment, and high carrier mobility were investigated[22,42], and systematical investigations were drove on predicting the crystal structure of the potential 2D allotropes in group-V elemental materials, as well as their average binding energy that indicates good stability and composability, which are presented in Fig. 2a, b, respectively. Herein and in the subsequent sections of this review, only α and β phases are summarized and discussed by considering reliable experimental results have been reported in these two phases of 2D forms. As seen from the side views in Fig. 2a, puckered monolayer formations can be observed in the α phase group-V elemental 2D materials (α-Vene), which have orthorhombic structure in space group *Cmca*, while wavy monolayer formations are existed in the β phase of group-V elemental 2D materials (β-Vene), which have rhombohedral structure in space group $R\bar{3}m$. In order to further demonstrate the atomic crystal structures of these two allotropes, selected area electron diffraction (SAED)

[1]Department of Applied Physics, The Hong Kong Polytechnic University, Hung Hom, Hong Kong, People's Republic of China. [2]The Hong Kong Polytechnic University Shenzhen Research Institute, Shenzhen 518057, People's Republic of China. ✉email: jh.hao@polyu.edu.hk

Published in partnership with FCT NOVA with the support of E-MRS

npj nature partner journals

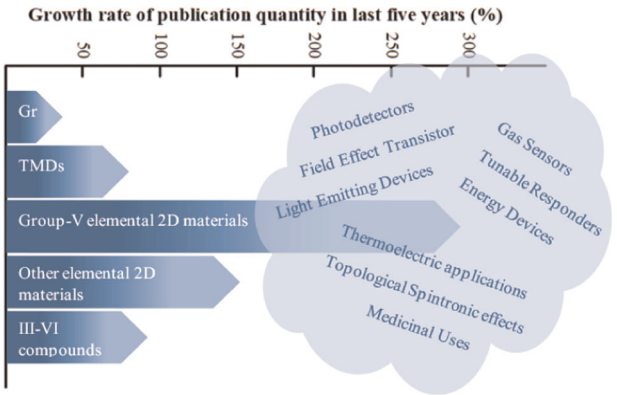


**Fig. 1 Comparison of the growth rate (percentage) of the quantity of the publications, regarding group-V elemental 2D materials with that of other 2D materials.** KEY WORDS: "Graphene", "$MoS_2$ or $WS_2$ or $MoSe_2$ or $WSe_2$ or $MoTe_2$", "Phosphorene or Black Phosphorus or Arsenene or Antimonene or Bismuthene", "Silicene or Germanene or Stanene or 2D Lead or Borophene or 2D single metal", "InS or $In_2S_3$ or GaS or InSe or $In_2Se_3$ or GaSe or GaTe". SEARCH ENGINE: Google Scholar.

patterns of α- and β-bismuthene as representative examples are shown in Fig. 2c, d, respectively[43].

The unique lattice structure of group-V elemental 2D materials brings challenges to the sample's synthesis and device's fabrication for further electrical characterizations. Similar to other classes of 2D materials, mechanical or solvent-based exfoliation methods have firstly been employed to synthesize group-V elemental 2D samples with high-quality beneficial for fundamental investigations, while other top-down methods like plasma-assisted strategies were also developed, but the scale of the obtained samples was still limited[6,10,20,25,44]. On the other hand, researchers have put their efforts on bottom-up methods using vapor deposition techniques, such as chemical vapor deposition, molecular beam epitaxy (MBE), and pulsed laser deposition (PLD). Till now, blue phosphorene, arsenene, antimonene, and bismuthine have already been synthesized via MBE or other vapor deposition techniques[45–49]. However, further researches on maintaining the stability of the as-prepared samples, including in situ encapsulation strategies and surface modifications, are still much needed. Particularly, feasible bottom-up synthesis process for BP recognized as the most promising member among group-V elemental 2D materials, remains unsuccessful.

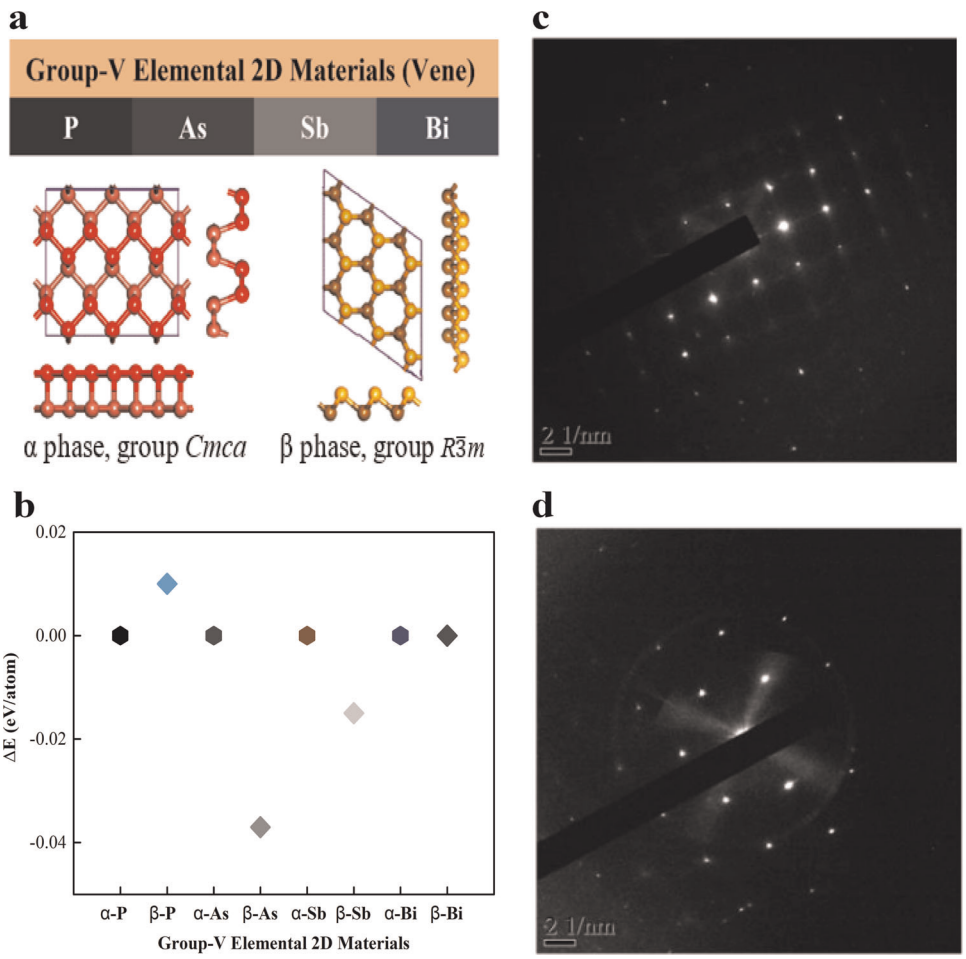


**Fig. 2 Crystal structures of group-V elemental 2D layers. a** Schematics of top views and side views (along *x*- and *y*-horizontal directions) of atomic crystal structures of α and β phase group-V elemental 2D materials (Vene). **b** Calculated average binding energies of α and β allotropes of all group-V elemental 2D materials, from which the related stability and composability can be acknowledged. **c**, **d** SAED images of α- and β-bismuthene, presenting one pseudo-cubic structure with four-fold symmetry in α-Vene and another hexagonal structure with typical six-fold symmetry in β-Vene, respectively. Images of **a** and **b** used with permission from John Wiley and Sons[22]. Images of **c** and **d** used with permission from John Wiley and Sons[43].

To date, a number of theoretical studies and experimental investigations have been carried out, which demonstrate rich properties in electrical transport, especially unique anisotropic electrical properties. Moreover, a broad range of tunable bandgap and promising topological edge transport states have been mined from the group-V elemental 2D materials[20–37,42,43,50–58]. Generally speaking, the investigations of electronic properties from these 2D elemental nanosheets have been rapidly expanded. Unfortunately, systematical reviews, discussions, and prospects on their electrical transport properties are still scarce. Hence, we provide an overview on the recent advances in group-V elemental ultrathin 2D layers with an emphasis on their intriguing electrical transport. 2D phosphorus, arsenic, antimony, and bismuth will be introduced in turn with summarization, analysis, and discussion, while innovative outlooks about future architecture of the related electronic applications are forecasted, with an expectation of broadening and deepening understanding of group-V elemental ultrathin 2D layers and affording helpful assistance for further explorations.

## PHOSPHORUS AND PHOSPHORENE

### Synthesis and fundamental electrical properties

Phosphorus has been proved to possess many allotropes like white, red, violet, black, and blue phosphorus, and the last two kinds of phosphorus have been received more attention in recent years because of their layered structure[25], which are named as phosphorene in few-layer state and show the promising peculiarity for the electronic device applications. Blue phosphorus, consisting of layered rhombohedral structure with hexagonal mesh plane that is twisted along the *z*-axis in monolayer, had been synthesized into few-layered structure through MBE technique[45,59,60]. However, blue phosphorene is quite unstable in atmospheric environment and thus reliable experiment reported so far is still a blank area, despite some predictions that unique electrical transport properties are expected[61]. Hence, developing in situ encapsulation strategies is a potential pathway forward for experimentally exploring electrical transport properties of blue phosphorene. In contrast, there are already tons of investigations that being carried out on the electrical transport of BP. Although BP in bulk state isolated early in the 20th century has proved to be the most stable form among the allotropes of phosphorus[62], it has only recently been rediscovered by exfoliating crystal into nanosheet with a few layers and applied to 2D research[63]. BP forms into a puckering-layer structure in monolayer with two-tier floors of atoms, which is quite different from other elemental 2D materials like Gr. Such a unique structure makes it a great challenge to obtain large-scale BP ultrathin samples through bottom-up synthesis process. To date, the commonly investigated BP samples are routinely synthesized by mechanical or solvent-based exfoliation, resulting in small scale from bulks[27,64]. Even so, those valuable electrical transport properties, including tunable bandgap with high carrier mobility, highly anisotropic transport properties, and topological characteristics, enable BP to serve as one of most promising 2D materials for nano-electronic and optoelectronic devices.

To explore the electrical transport properties of BP, angle-resolved photoemission spectroscopy (ARPES) technique is applied to verify its electronic band structure. The experimental results carried out by Li et al. are consistent with the theoretical calculation (Fig. 3a)[63], clearly showing a direct bandgap of ~0.2 eV. Subsequently, Liu et al. observed the tunable energy bandgap with significant layer dependence in few-layer BP (ref. [27]), and a bandgap of ~1.45 eV was observed from the monolayer black phosphorene flake through photoluminescence (PL) measurement, as shown in Fig. 3b. The presence and tunable feature of direct bandgap make BP become a strong competitor to Gr with absence of bandgap, as well as TMDs usually exhibiting indirect bandgap in few layers. Hence, such excellent transport properties of BP may show more potential in future semiconductor applications.

Compared to the two conventional 2D materials, namely Gr and $MoS_2$ (or other TMDs), BP is a comprehensively dominant choice for 2D electronic devices because of its high charge-carrier mobility and current-switching ratio to be utilized as the channel material in field-effect transistors (FETs)[65]. In 2014, the p-type transport characteristics with high charge-carrier mobility (up to 1000 $cm^2V^{-1}s^{-1}$) were observed from the switching behavior of black-phosphorus-based FETs (ref. [27]). It is one of considerable advantages over the TMDs, principally benefited from its ultra-low deformation potential value (~0.15 ± 0.03 eV) of the forbidden band edge along the transportation direction[32,66]. As presented in Fig. 3c, d, thickness (layer) and temperature dependence of carrier mobility, and other electrical transport properties are further demonstrated, which could be attributed to the interlayer coupling in phosphorene[24,27,63,67–71]. Field-effect-based carrier mobility values of 984, 197, and 55 $cm^2V^{-1}s^{-1}$ were obtained from three BP samples with different thickness of 10 (black line), 8 (red line), and 5 (green line) nm, respectively. Because of the instability of few-layer BP in the atmosphere, researchers further developed encapsulation strategies by using dense oxide layer like $AlO_x$ or chemical macromolecular layer like aryl diazonium molecules. As a result, covalent functionalization and passivation on the as-exfoliated BP flakes significantly extend the service life of the BP-based devices for maintaining the original electrical transport properties of BP in natural environment[72,73]. However, due to the difficulty of obtaining crystalline BP by bottom-up process, only exfoliated BP flakes had been employed to make FETs for demonstrating their electrical performance so far. On the other hand, amorphous BP ultrathin films have first been fabricated through PLD by our team[74], and subsequently unique carrier transport features with astonishingly high exciton diffusion coefficient and long exciton lifetime were observed in the novel samples by Zhao et al., as shown in Fig. 3e, f (ref. [75]). Hence, it implies that employing physical vapor deposition might be promising to overcome the hurdle on the way to achieving large-scale BP samples, and accordingly further explorations on their electrical transport properties are expected. Additionally, ultrafast and efficient electrical transport is found from crystalline monolayer to amorphous BP ultrathin layer, which opens up new avenues for BP applications[76]. Accordingly, the study of the electrical transport on the integrated structures, such as heterojunction or vertical transistor is another prospective topic for further investigations[77,78]. Based on these findings, it implies that careful design with considerations of unique responses or effects resulted from the interface or interlamination of phosphorene and other 2D materials is required for the related electronic applications in the future.

### Highly anisotropic transport properties

Because of the unique puckering structure, lower effective masses take shape along the armchair direction, forming remarkably anisotropic features in electrical transport of 2D BP that greatly distinguishes it from other 2D materials, so as to attract lots of interest[33,34,68,79–83]. Angular-dependent electrical transport properties, including drain current and transconductance could be clearly observed as shown in Fig. 3g (ref. [27]), and the specially designed device structure with eight metal contacts in a circle with 45° as interval is shown in the inset. The in-plane anisotropic feature can also be investigated from the planar view of the squared electron wavefunction (Fig. 3h), which distinctly demonstrates that carriers are more preferable to transport along the *x*-direction than *y* (ref. [81]). It is intriguing to refine the on-state output characteristics for the devices with channel length in atomic level under quantum tunneling effect[84,85]. Besides,

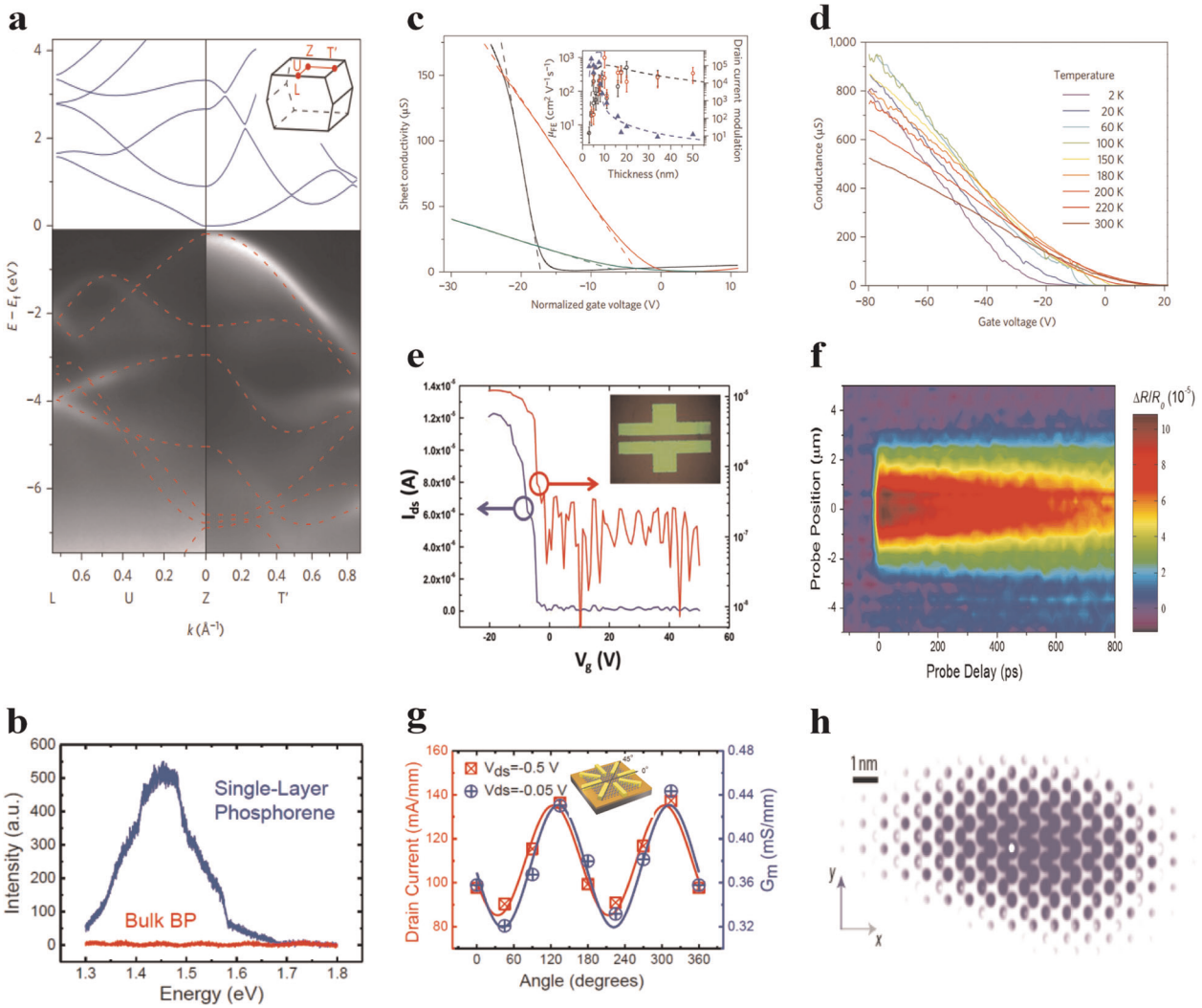


**Fig. 3 Fundamental electrical transport properties of BP. a** Calculated (top) and ARPES-mapped (below) results regarding the band structure of bulk black phosphorus. **b** PL spectra for monolayer phosphorene and bulk black phosphorus samples. The bandgap of monolayer black phosphorene can be concluded to be ~1.45 eV accordingly. **c**, **d** Thickness (layer) and temperature dependence of the conductivity measured as a function of gate bias, respectively. **e**, **f** Carrier transport and exciton diffusion characteristic of 2-nm amorphous BP ultrathin film, respectively, demonstrating through FET transfer curve and spatiotemporal differential reflection signal. **g** Angular-dependent performance on drain current and transconductance of the eight-electrodes devices based on few-layer black phosphorus. The inset shows schematic of the new-designed device with eight electrodes in a circle for investigating the anisotropy transport features of BP. **h** Planar view of the squared electron wavefunction for the exciton at ground state in the single-layer black phosphorus. Images of **a**, **c**, and **d** used with permission from Springer Nature[63]. Images of **b** and **g** adapted with permission from ref. [27] copyright 2014, American Chemical Society. Image of **e** used with permission from John Wiley and Sons[74]. Image of **f** © IOP Publishing. Reproduced with permission from ref. [75]. All rights reserved. Images of **h** used with permission from Springer Nature[81].

interesting transport property with quasi one-dimensional feature could also be defined, which shows the potential in the development of functional electronic devices[39].

Moreover, Pumera et al. studied the strongly anisotropic magnetic and electrical transport properties on the edges of few-layer black phosphorus edges in detail[79]. In Fig. 4a, b, special molecular probes were used to show the considerable difference in the conductivity, reflecting the electron transfer characteristics of 2D black phosphorus along perpendicular (base-plane) and parallel (edge-plane) directions. The works extend the study of the anisotropic transport properties of 2D BP to the out-plane region and offer more possibilities to the design of novel devices.

## Strain and electric field tuning on electrical transport properties

In addition to the intrinsic properties mentioned earlier, it is found that external modulation methods, such as applied strain or electric field, can also affect the electrical transport properties of BP, including energy bandgap and carrier migration by the zigzag edge, even leading to a topological phase transition[34,35,80,86–88]. As shown in Fig. 4d, e, applying strain is found to have appreciable influence on tuning the charge-carrier transport properties of phosphorene nanoribbons (PNR), in which the anisotropic properties can also be observed. In the PNR with zigzag edge (*z*-PNR), the researchers observed the most significant tuning effect on the energy bandgap and the effective mass of electrons and holes[80]. Remarkably, a critical transformation can be observed on the effective mass of charge carriers when a certain amount of positive pressure is applied, and this will play an important role in tuning the electrical transport property of BP. On the other hand, by means of optical techniques to measure the infrared optical response of BP flakes, electric field was found to possess detectable gating effects on the band structure and exciton

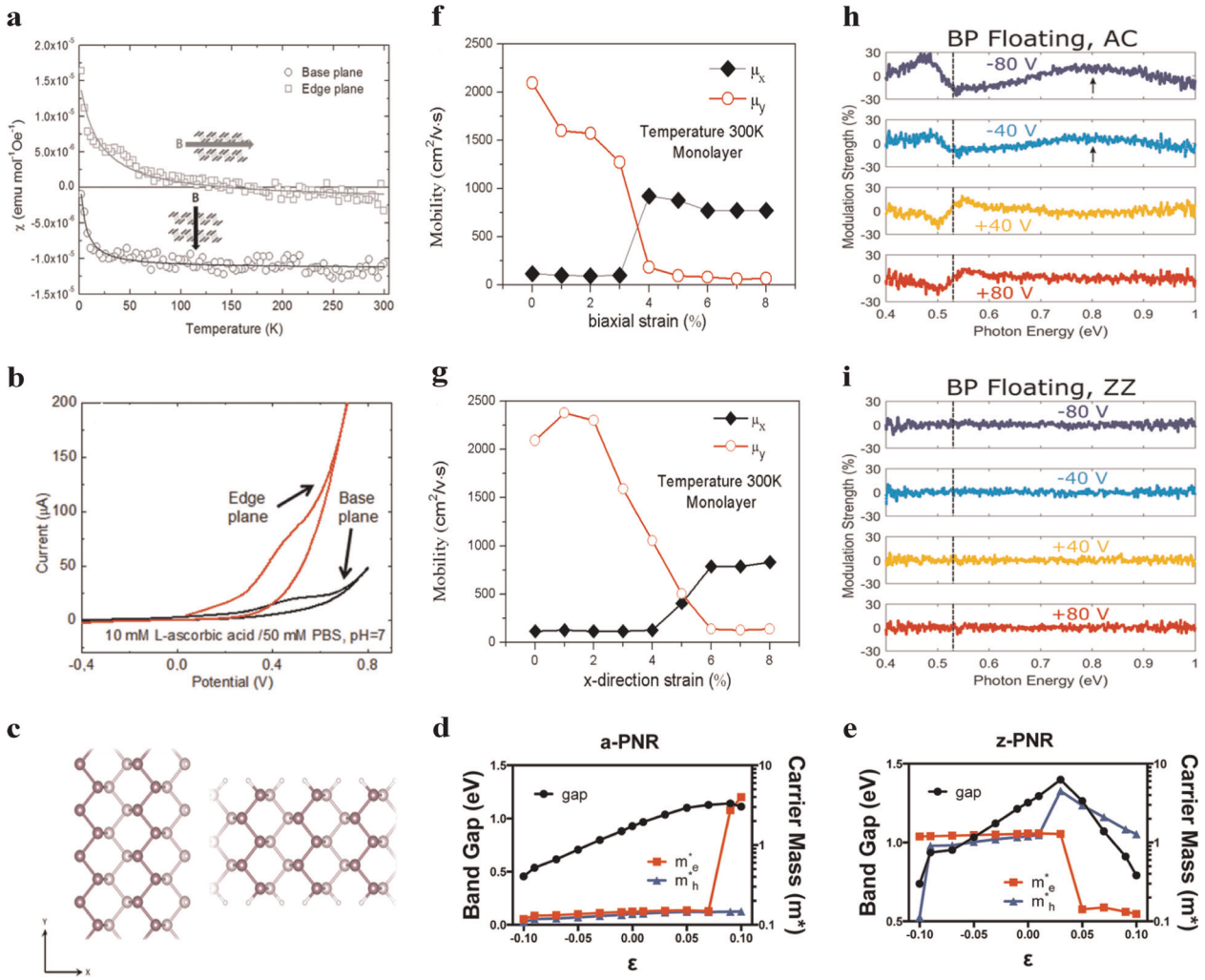


**Fig. 4 Controllable and tunable characteristics of BP under external potential field. a** Different level of magnetic susceptibility conducted by incongruous external field along perpendicular and parallel direction. **b** One example for demonstrating the discrepant active behavior of biosensing reaction along perpendicular and parallel direction of few-layer black phosphorus. **c** Schematic structures of *z*-PNR (left) and *a*-PNR (right), indicating PNRs with typical layer-edge types and electrical transport directions of zigzag and armchair, respectively. **d**, **e** Transformation behaviors of energy bandgap and effective carrier masses under applied strain (*ε*) in *a*-PNR and *z*-PNR, respectively. **f** Electron mobilities along zigzag ($\mu_x$, black curve) and armchair ($\mu_y$, red curve) directions in single-layer black phosphorus at room temperature under varied in-plane biaxial strain. **g** Same research objectives as **f**, under varied uniaxial strain along *x*-direction. **h**, **i** Electric field tuning effects of BP oscillator strength that show light polarized along armchair (AC) axis and zigzag (ZZ) axis, respectively. Images of **a** and **b** used with permission from John Wiley and Sons[79]. Images of **c**–**e** adapted with permission from ref. [80] copyright 2014, American Chemical Society. Images of **f** and **g** adapted with permission from ref. [34] copyright 2014, American Chemical Society. Images of **h** and **i** adapted with permission from ref. [92] copyright 2019, American Chemical Society.

generated behaviors of BP (refs [89,90]), which was further attributed to the giant Stark effect through low-temperature scanning tunneling microscopy (STM) measurements[91]. Moreover, the anisotropic features could be engineered by modulating either strain or electric field. As seen from the schematic and results in Fig. 4f, g, spatial preference of electron mobilization would have a 90° rotation while either certain *x*-direction uniaxial or in-plane biaxial strain was applied[34]. Figure 4h, i exhibits the tuned performance of extinction from BP flake under specific carrier floating constant, from which two tunable features are detectable along armchair axis, but no tunability can be found along zigzag axis[92]. Accordingly, a shutdown effect on one-dimension could be created, and hence some applications based on switching transmission direction as well as the on/off state along planar axis are expected, which are valuable for further applications, such as advanced optical devices or large-area electronic integrations with controlled electron migration along specific uniaxial direction in multidimensional systems.

## ARSENIC AND ARSENENE

### Synthesis and fundamental electrical properties

Arsenic has two layered allotropes, where black arsenic (α phase) and gray arsenic (β phase), and layered gray arsenic are known to be existed in nature[93–95]. Next to layered phosphorene, arsenene inspires great research interest in the field of 2D materials. Many researches have been put forward on exploring the electronic structure of 2D arsenic, and it is found that α-arsenene has a direct bandgap within a desired range, which is expected to be an ideal semiconductor[21,96]. Furthermore, ultra-high hole mobility exceeding 14,000 $cm^2V^{-1}s^{-1}$ was predicted in α-arsenene, showing its potential as donors in solar cell[97]. Similar to other 2D materials,

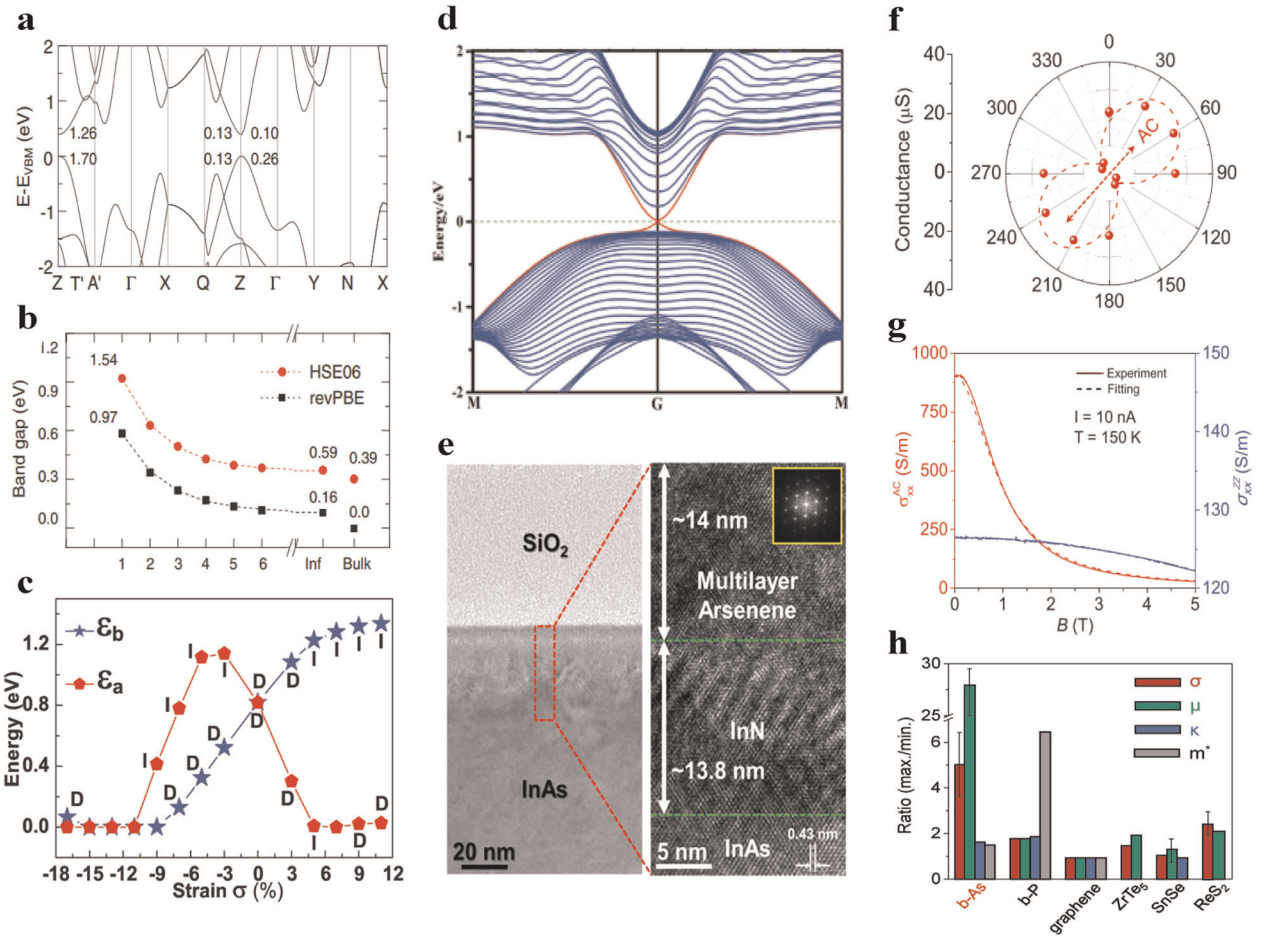


**Fig. 5 Electrical transport properties of arsenic ultrathin 2D layer. a** Calculation of the band structure for orthorhombic arsenene, showing its direct bandgap. **b** Layer dependence of the energy bandgap of α-arsenene. **c** Variation of the bandgap of α-arsenene, including direct (marked by letter D)/indirect (marked by letter I) energy band, as a function of the applied strain along zigzag ($\varepsilon_a$) and armchair ($\varepsilon_b$) directions. **d** The tuning tendency of the electronic structure for β-arsenene nanoribbon with zigzag edge, constructing with a 11.7% tensile strain, from which the helical edge states could be prospected at G point. **e** Cross-sectional transmission electron microscope images of the multilayer arsenene synthesized by plasma-assisted process. **f** Angle-dependent appearance on electrical conductance of α-arsenene, exhibiting the preferred transportation along armchair (AC) direction. **g** Magnetic-field-dependent conversion of longitudinal conductivity $\sigma_{xx}$ along armchair (AC) and zigzag (ZZ) directions. **h** Comparison of the in-plane anisotropic electrical transport properties of α-arsenene and some other 2D materials. Images of **a** and **b** adapted with permission from ref. [21] copyright (2015) The Japan Society of Applied Physics. Image of **c** republished with permission of Royal Society of Chemistry, from ref. [96]; permission conveyed through Copyright Clearance Center, Inc. Image of **d** republished with permission of Royal Society of Chemistry, from ref. [100]; permission conveyed through Copyright Clearance Center, Inc. Image of **e** adapted with permission from ref. [51] copyright 2016, American Chemical Society. Images of **f**–**h** used with permission from John Wiley and Sons[101].

layer (thickness) and temperature dependence of electrical transport properties can be observed in 2D layered arsenene (Fig. 5a, b)[21,98,99]. Moreover, patterning and strain modification can produce significant effects on the electrical transport of layered arsenene[96,100]. Ma et al. investigated the transformation behaviors of energy bandgap of α-arsenene under the uniaxial strain along zigzag ($\varepsilon_a$) and armchair ($\varepsilon_b$) directions, as shown in Fig. 5c (ref. [96]). In addition to the variation in the bandgap magnitude that results in the transformation from semimetal to semiconductor, the intrinsic direct energy band of α-arsenene can be modified to indirect one under certain pressure conditions, which could satisfy the requirements for further designs of strain-tuned devices. In addition, with the assistance of density functional theory calculations, it is found that suitable tensile-strain modulation can lead to a transformation in honeycomb arsenene, as illustrated in Fig. 5d, and topological insulator phenomenon is observed in the 2D material at room temperature[100].

In addition to traditional exfoliation methods, Tsai et al. presented a bottom-up preparation technique, i.e., the plasma-assisted process, to synthesize multilayer arsenene on InAs, as shown in Fig. 5e (ref. [51]). In this fabrication, nitrogen ions were introduced into InAs single crystal by heating treatment, where the N ions could react with In ions, and As was squeezed out from arsenene layers on the surface. Remarkably, the thickness of the as-prepared arsenene can be modulated by controlling the reacting time of plasma, which largely provides possibilities for further device's design. What should be mentioned is that both α-arsenene and β-arsenene are more stable in natural environment than BP and blue phosphorene, which makes arsenene a good alternative to compete with phosphorene.

## Anisotropy in electrical transport properties of α-arsenene

Both α-arsenene and β-arsenene are naturally 2D materials with layered structure. Of the two, α-arsenene has a BP-like puckering structure, and accordingly a valuable in-plane anisotropy in

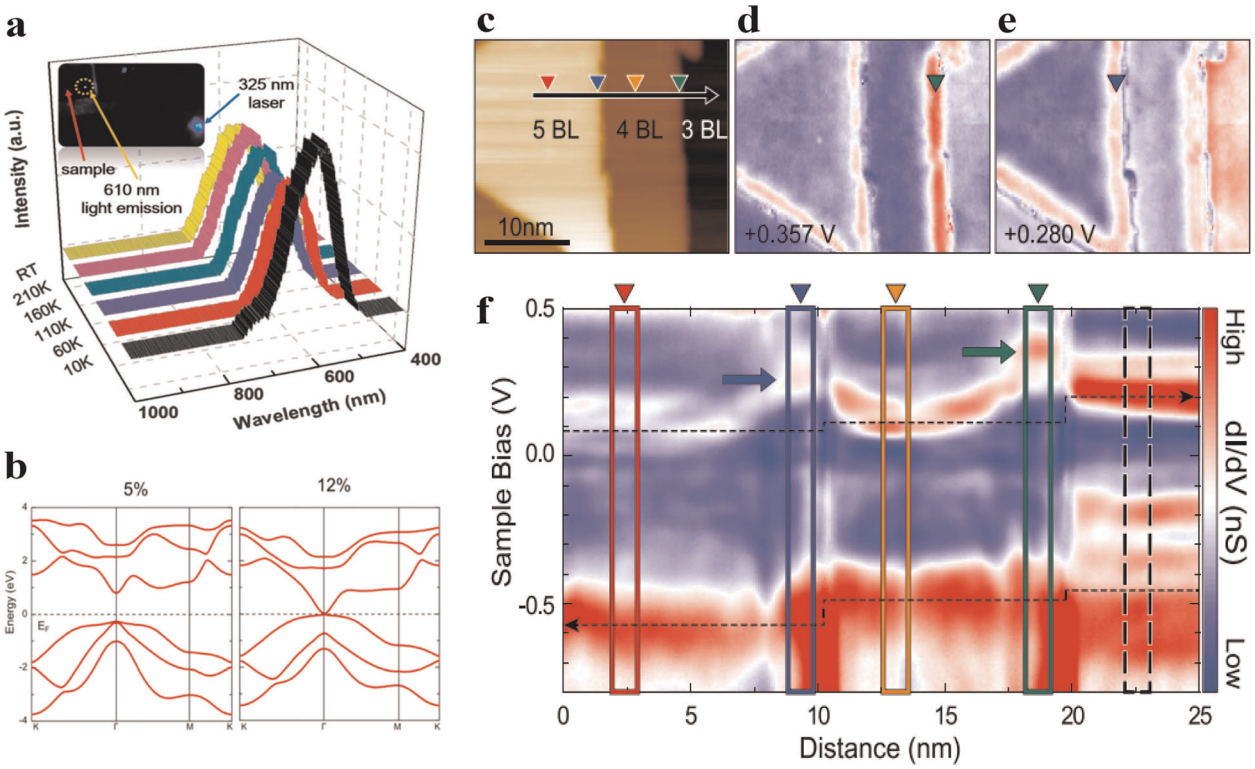


**Fig. 6 Electrical transport properties of antimony ultrathin 2D layer. a** Photoluminescence spectra of 2D antimonene at different temperatures, showing its desirable bandgap nature. **b** Electronic band structures of monolayer β-antimonene under 5 and 12% biaxially tensile strains, respectively. **c** Topography imaging of antimonene islands obtained by STM, exhibiting the edges of five-layer sample and 4-layer sample. The related *dI/dV* mapping results are shown in **d** with +0.357 V and **e** with +0.280 V as bias. **f** Bias-dependent line scanning for *dI/dV* obtained along the arrow-indicated direction in **c**. Four colored rectangles are corresponding to relevant symbol in **c**. Image of **a** republished with permission of Royal Society of Chemistry, from ref. [52]; permission conveyed through Copyright Clearance Center, Inc. Image of **b** adapted with permission from ref. [113] copyright 2015, American Chemical Society. Images of **c**–**f** used with permission from Springer Nature[111].

phonon properties and electrical transport properties are expected[101–103]. As shown in Fig. 5f, angle-dependent appearance is clearly observed on the conducting property of α-arsenene. Except for the intrinsic performance, the introduction of external magnetic field would further affect the anisotropy on the electrical conductance of α-arsenene. Figure 5g exhibits the magnetic-field-dependent variation of longitudinal conductivity $\sigma_{xx}$ along armchair and zigzag directions, from which the enormous bondage is occurred for the carrier transport along armchair direction and furthermore the preferred orientation of carrier transport is shifted under high magnetic field. The results offer an opportunity to conceive relevant magnetic control devices and applications.

Compared to other 2D materials like BP and Gr, α-arsenene shows more noteworthy anisotropic transport properties[101], including thermal conductivity $\kappa$, electrical conductance $\sigma$, mobility $\mu$, and magnetic-field modulated longitudinal conductivity $\sigma_{xx}$ and transverse conductivity $\sigma_{xy}$, as summarized in Fig. 5h. It should be emphasized that both electrical conductance $\sigma$ and mobility $\mu$ are the two important parameters of the materials that are considered as constituent parts in electronic devices. α-Arsenene has more distinct anisotropic properties than BP, therefore it might be a more promising materials in many electronic applications, such as crystal orientation-controlled devices and multidimensional integration applications.

## ANTIMONY AND ANTIMONENE

### Synthesis and fundamental electrical properties

Antimony naturedly shows metallic properties in its bulk state, which is widely used in battery applications by alloying it with lead and tin[104]. Recently, β-antimony was reported to possess layered structure, and accordingly many novel features are expected in few-layer antimonene[53,93,105]. When being exfoliated down to a monolayer state, antimonene exhibits a semiconductor behavior with an indirect bandgap up to 2.28 eV according to the theoretical prediction[22]. This is a quite suitable magnitude of bandgap that provides abundant possibility for the further development of optoelectronic devices operating in visible spectra. Afterward, a series of theoretical investigations were carried out in exploring the intrinsic and modulated transport properties of 2D antimonene, including defect movement, spin–orbit coupling effect, thermoelectric conductivity and so on[93,106–110], and these rich and valuable features make the study of 2D antimonene become a new research hotspot.

Except for the mechanical exfoliation methods, 2D antimonene with layered structure has been successfully fabricated on different substrates, including mica and InSb by bottom-up methods[48,52,54,111,112], and a bandgap of larger than 2 eV was experimentally observed, as shown in Fig. 6a. Moreover, similar to arsenene, few-layer antimonene shows relatively high stability in air, showing its strengths in electronic application[105]. MBE and other bottom-up synthesis methods have been employed for preparing large-scale antimonene[48,49]. Nevertheless, similar to few-layer $MoS_2$ and other TMDs, one weakness for antimonene is resulted from its intrinsic indirect bandgap that might restrict optoelectronic device application based on the 2D layer. Some researches predicted that strain engineering would generate remarkable effects on the electrical transport properties of 2D antimonene[42,113–115]. According to the theoretical study on tuning bandgap[113], a biaxially tensile strain of 5% would turn the

bandgap of β-antimonene into direct at Γ point, in comparison with the indirect one at the initial equilibrium position. The band closure phenomenon is occurred when the strain of 12% is applied, as seen in Fig. 6b. This is of significance since the work promises optoelectronic applications based on the attractive semiconductor properties from the 2D antimonene with an appropriate bandgap. Nevertheless, there is a lack of experimental evidence to prove the prediction so far.

### Topological phase transition and quantum spin Hall edge states

In general, those elements in the lower position of the periodic table or their compounds usually have distinct topological insulation (TI) features. Therefore, antimonene and bismuthene (to be discussed in the latter section) are expected to show unusual electrical transport properties attributed to their topological phase transition and the quantum spin Hall edge states[107,108,111,114]. As shown in Fig. 6c, Kim et al. synthesized antimonene samples with three to five layers on $Bi_2Te_2Se$ substrate with sharp edge between different layers, and further carried out investigations on the topological phase transition and quantum spin Hall edge states through STM measurement[111], from which the plump and sturdy edge electronic states with substantial modulation effect could be observed on the step edges of five and four bilayers (BL, referring to one antimonene layer with double atomic-layer) samples. Large edge-state effect on prominent *dI*/*dV* energies is evident, as shown in Fig. 6d, e. Accordingly, special channels for electrical transport are opened up, and controllable by an external electric field (Fig. 6f).

The existence of these intrinsically localized edge channels for electrical transport may provide additional influences on the performance of nano-devices, and hence 2D TI features are expected to be more predominant and worth studying than 3D TI features in bulk materials on account of the localized conduction directions only in 2D region[116], which results in weakened interference from the nonmagnetic backscattering.

## BISMUTH AND BISMUTHENE

### Synthesis and fundamental electrical properties

Except for layered α-bismuthene that has been predicted but not yet been experimentally proven, β-bismuthene, the confirmed 2D layered state of bismuth, is composed of a wavy structure in 2D hexagonal lattice like blue phosphorene, gray arsenene, and antimonene. However, only indirect and small bandgap up to ~0.3 eV can be observed in bismuthine, which might limit its applications in electronic field[117,118]. But surprisingly, bismuthene is relatively stable in general environments, and is not relatively difficult to be controllably grown into large-scale sample. Hence, bismuthene is more possible to be used in complex device structures with multiple manufacturing processes[119]. Accordingly, there are lots of interests to investigate the electrical transport properties of bismuthene[120–126]. Our group fabricated layered bismuthene in centimeter scale with two different orientations, (110) and (111) by PLD (ref. [43]). Through controlling the processing temperature during PLD process, the thickness-dependent bandgap transformation was observed, from which a small bandgap of ~0.2 eV is evident in the 1-nm ultrathin bismuth film (Fig. 7a). As shown in Fig. 7b, it is interesting to note that the ultrathin (110)-orientated bismuthene shows electric insulating, while the few-layer (111)-orientated bismuthine shows layer-dependent bandgap transformation and a p-type semiconductor characteristic with a relative high carrier mobility of ~220 $cm^2V^{-1}s^{-1}$. In fact, such a high mobility is in prospect, while a carrier mobility in the level of $10^4$ $cm^2V^{-1}s^{-1}$ is observed in a thicker bismuth film[127], which shows considerable capacity for further development of related electronic devices, such as logic transistors. Consequently, the above works on amorphous BP and bismuthene done by our group imply that PLD is an alternative technique to synthesize 2D materials[128,129], including group-V elemental 2D materials.

In addition, due to the light effective carrier mass and large mean free path in the lattice structure, bismuthene is expected to possess particular electrical transport properties related to finite-scale effects when modulating by vigorous magnetic field[130–133]. From the investigations on single-crystal bismuth thin-film, large magnetoresistance (MR) effect is found to exhibit its dependence on the detecting angle and the magnitude of external magnetic field. Additionally, it is found that controllable magnetic-enabling transformation of the sample has an influence on its electrical transport properties (Fig. 7c), although it is not yet experimentally evident in few-layer bismuthine[130,131]. Interestingly, such MR phenomenon has already been observed in other classes of 2D materials like TMDs via ferromagnetic gating, which is reported by our group[134]. It is intriguing and attractive to understand the semi-metallic and high mobility nature of bismuthene, and therefore new concept designs could be conceived by using noncontact modulation strategy.

### Topological transport states with edge-dependent effect

As mentioned in the earlier section, 2D TI effects are worthy research toward next-generation electronic devices. In fact, due to the odd number of spiral edge-state twains and the nontrivial topological exponents, the topological electrical transport properties in bismuthene are more anticipated compared to other 2D materials[58,116,117,122–124,135–138]. Typically, through STM technique, extensive investigations on the topological transport properties of bismuthene had been conducted by Drozdov et al., and a series of edge states of bismuthene are decoupled from the formations of the bottom bismuth crystal acting as the substrate[137]. As shown in Fig. 7d, there are two different types of edges in monolayer bismuthene flakes, namely type A and B, and disparate characteristics of electrical transport can be observed along different type of edge and on the surface (Fig. 7e). It is concluded that the electrical transport properties are able to be engineered on type A edge of bismuthene, and the singularity inherent to one-dimensional carrier transport systems are proved to be existed continuously with strong edge dependence. On this basis, what can be expected is that, some open-to-close reversals or loops are able to be designed and realized for widespread electronic applications based on few-layer bismuthene.

## CONCLUSIONS AND PERSPECTIVES

In summary, 2D group-V materials, including phosphorene, arsenene, antimonene, and bismuthene, are all capable of showing unique and promising electrical transport properties that offer a novel research platform for exploring physical properties in atomic level and broadening perspectives of nano-device research. Particularly, in comparison with other elemental ultrathin 2D layers (e.g., Gr, borophene, and germanene) showing semi-metallic or metallic feature, elemental 2D group-V materials are proved to be potentially semiconductors with suitable bandgaps that can be tuned over a wide range from a few tenths to larger than 2.5 eV. Moreover, this class of 2D materials possesses relatively high carrier mobility to fulfill the requirements of high-performance electronic devices. For each group-V elemental 2D material, we have introduced its crystal structures and synthesis strategies in this article. Regarding fundamental properties, these elemental ultrathin 2D layers show valuable semiconducting behaviors, layer- (thickness-), and temperature-dependent features with tunable bandgap and relatively high carrier mobility.

Table 1 summaries electrical transport properties of phosphorene, arsenene, antimonene, and bismuthene, which would benefit for selecting appropriate elemental ultrathin 2D layers in both

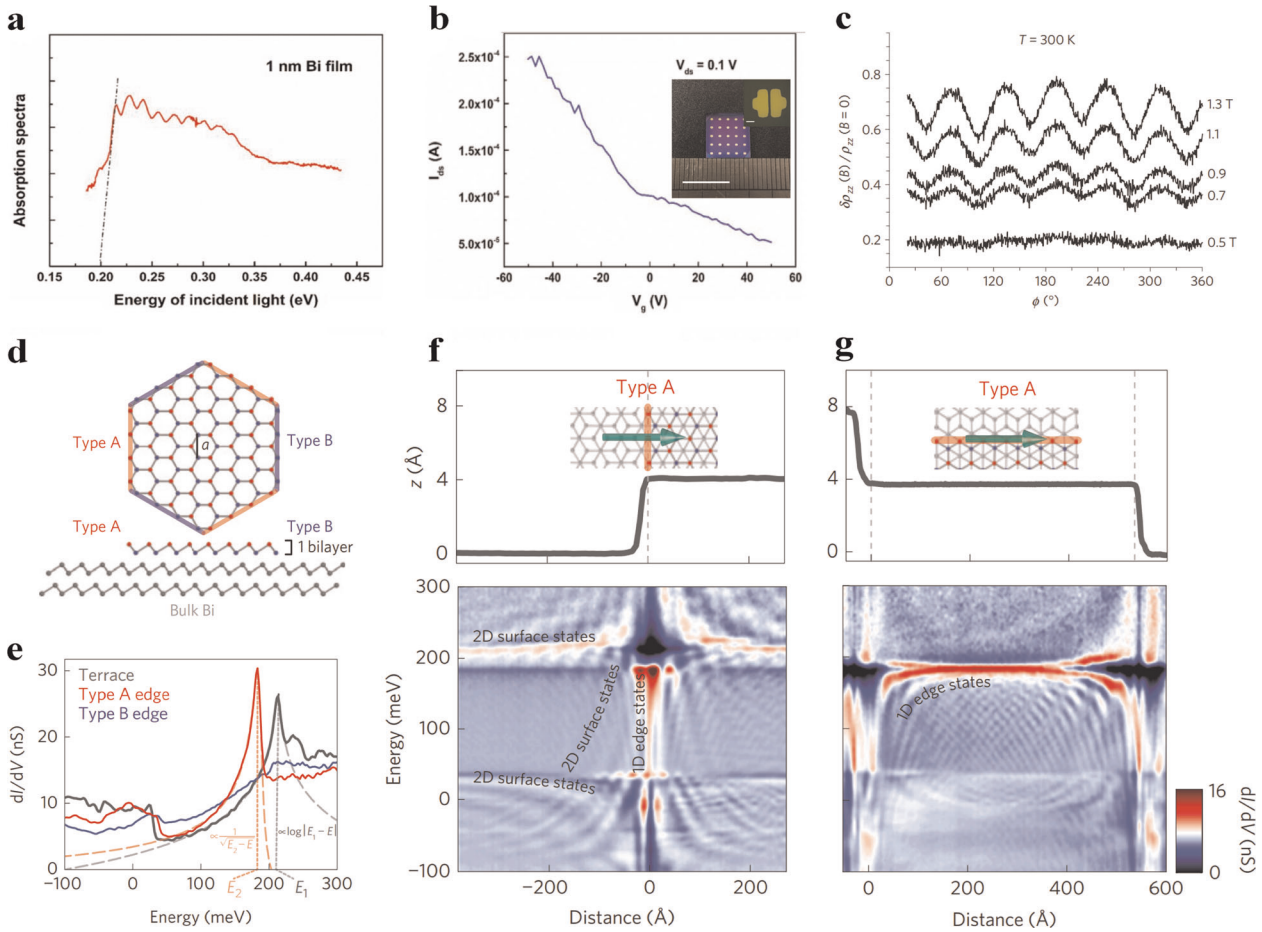


**Fig. 7 Electrical transport properties of bismuth ultrathin 2D layer. a** Absorption spectrum for 1-nm bismuthene sample, showing tiny bandgap of ~0.2 eV. **b** Typical p-type transferring characteristic examined from one 10-nm-Bi-based FET. The inset shows 25 FETs evenly distributed across the centimeter plane of Bi ultrathin film. **c** Magnetic resistance performance of bismuth monocrystal with significant angular dependence that are investigated under different magnitudes of external magnetic field. **d** Schematics of two different edge types in bismuthene monolayer, showing by planar view and side view. **e** Point spectroscopy spectra of the *dI*/*dV* value as a function of the energies. Red, blue, and gray line are referred to the measurements along type A edge, along type B edge, and on the uniform surface, respectively. **f**, **g** Topographic line-cut feature and spectroscopy with energy line-scanning across and along the type A edge, respectively, which clearly exhibited the 1D edge state. Images of **a** and **b** used with permission from John Wiley and Sons[43]. Image of **c** used with permission from Springer Nature[131]. Images of **d**–**g** used with permission from Springer Nature[137].

**Table 1.** Summary of electrical transport properties in group-V elemental ultrathin 2D layers.

| Materials | Typical bandgap | Typical mobility | Some electrical transport properties |
|---|---|---|---|
| Phosphorus and phosphorene | ~1.8 eV<br>Direct | A few thousands | High mobility with direct bandgap<br>Highly anisotropic transport properties<br>Strain tuning properties |
| Arsenic and arsenene | ~ 2.3 eV<br>Direct | A few hundreds and more | Direct and wide bandgap<br>Anisotropic transport properties in α-As |
| Antimony and antimonene | ~2.28 eV<br>Indirect | A few hundreds and more | Topological phase transition properties<br>Quantum spin Hall edge states<br>Stain tuning into direct wide bandgap |
| Bismuth and bismuthene | ~ 0.3 eV<br>Indirect | A few hundreds to a few thousands | Light effective carrier mass and large mean free path<br>Magneto-electronic properties<br>Topological transport properties and 1D edge states |

fundamental study and device design. As the first discovered and most studied member, phosphorene shows a very attractive characteristic of high carrier mobility with direct bandgap. Furthermore, the anisotropic nature of BP is noteworthy for further explorations. The study might include elaborate design and construction of one-dimensional variations or combinations on 2D plane. Such a promising structure is helpful to boost the 2D electronic research in this field, but it still lacks comprehensive

study up to now. Furthermore, strain engineering has extensively been used for tuning elemental Gr and other 2D material's properties[139,140]. Similar to these studies, applying strain is capable of producing more significant effect on BP when considering its excellent electrical transport characteristics. It should be pointed out that the intrinsic instability of phosphorene still causes great restrictions for its further investigation, and therefore more explorations of materials processing, such as optimizing growth, post-processing, capping methods are indispensable, aiming at achieving large-area samples with high crystalline quality, and promoting potential application of BP.

In terms of the other elemental ultrathin 2D layers in group-V, some intriguing electrical transport properties have been summarized and discussed. However, an in-depth understanding of these properties is still insufficient. Arsenene has a wide and direct bandgap, which could offer some merits in the design of optoelectronic device. In addition, α-arsenene has anisotropic transport properties like BP. Therefore, α-arsenene could also play a similar role in relevant applications with the reference of BP, though these applications of arsenene could be limited by its carrier mobility. Unlike phosphorene and arsenene, antimonene shows an indirect bandgap, but existing investigations have proved that applying strain can not only enlarge its bandgap but also induce a transformation from indirect to direct energy band. These reported results make it still desirable for optoelectronic applications by considering its appreciable stability and compatibility with mature technology on large-area preparation. In addition, the quantum spin Hall edge states and topological electrical transport properties are expected to be achieved in another group-V elemental 2D material, bismuthene, which may pave the way for novel applications based on the heterostructure design. Although it has a small bandgap of ~0.3 eV, bismuthene has been attracting more and more research interest because of its outstanding electrical transport properties. One of the most worth-mentioning features is that bismuthene can be successfully fabricated on functional substrates like SiC (0001), and accordingly it is expected to realize high-temperature quantum spin Hall structure. Besides, it is noticeable that the magnetically tuned electrical transport properties are useful for conceiving novel devices, such as noncontact regulator. Importantly, for all of the group-V elemental 2D materials, the strategy of modification and doping shows a promise in tuning their electrical transport properties, attributed from the unique puckering or wavy structures in their monolayers[141–143].

Although group-V elemental ultrathin 2D layers have been proved to own many intriguing and useful electrical transport properties, a major hurdle to be overcome is to develop synthesis strategy for preparing wafer-scale and ultrathin layers, which can adapt to various device applications. Especially for phosphorene, because of its unparalleled carrier transport capability with excellent semiconductor features, searching an effective synthesis method capable of producing high quality and stable BP are in urgent need for facilitating its further development. Meanwhile, there is still much room for in-depth studies on applying these unique properties, such as remarkable layer-dependent phenomena, anisotropic feature, interlayer edge effect, and electrical control of neutral and charged excitons[144] to group-V elemental 2D material-based device's construction. In addition, expanding the research scope of materials technology, including doping, alloying, and surface or interlayer modification of this family of 2D materials is one of future research directions that deserves further studies. To sum up, we have provided an overview on recent advance of electrical transport in phosphorene, arsenene, antimonene, and bismuthene, aiming at promoting the research field and improving understanding of these group-V elemental ultrathin 2D layers, which have just been entering in the incipient stage. It is hoped that the development of synthesis strategy and the exploration of heterostructure device structure would pave the way for many promising group-V elemental ultrathin 2D layer-based electronic and optoelectronic applications in the future.

## DATA AVAILABILITY

The authors declare that the data supporting the findings of this study are available within the paper.

Received: 22 January 2020; Accepted: 6 March 2020;
Published online: 27 March 2020

## REFERENCES

1. Novoselov, K. S. et al. Electric field effect in atomically thin carbon films. *Science* **306**, 666–669 (2004).
2. Xia, F., Wang, H., Xiao, D., Dubey, M. & Ramasubramaniam, A. Two-dimensional material nanophotonics. *Nat. Photon* **8**, 899–907 (2014).
3. Franklin, A. D. Nanomaterials in transistors: from high-performance to thin-film applications. *Science* **349**, aab2750 (2015).
4. Chhowalla, M., Jena, D. & Zhang, H. Two-dimensional semiconductors for transistors. *Nat. Rev. Mater.* **1**, 16052 (2016).
5. Tan, C. et al. Recent advances in ultrathin two-dimensional nanomaterials. *Chem. Rev.* **117**, 6225–6331 (2017).
6. Kong, X., Liu, Q., Zhang, C., Peng, Z. & Chen, Q. Elemental two-dimensional nanosheets beyond graphene. *Chem. Soc. Rev.* **46**, 2127–2157 (2017).
7. Akinwande, D., Petrone, N. & Hone, J. Two-dimensional flexible nanoelectronics. *Nat. Commun.* **5**, 5678 (2014).
8. Jie, W., Yang, Z., Bai, G. & Hao, J. Luminescence in 2D Materials and van der Waals Heterostructures. *Adv. Opt. Mater.* **6**, 1701296 (2018).
9. Balendhran, S., Walia, S., Nili, H., Sriram, S. & Bhaskaran, M. Elemental analogues of graphene: silicene, germanene, stanene, and phosphorene. *Small* **11**, 640–652 (2015).
10. Zhang, Y., Rubio, A. & Lay, G. L. Emergent elemental two-dimensional materials beyond graphene. *J. Phys. D. Appl. Phys.* **50**, 053004 (2017).
11. Wang, Q. H., Kalantar-Zadeh, K., Kis, A., Coleman, J. N. & Strano, M. S. Electronics and optoelectronics of two-dimensional transition metal dichalcogenides. *Nat. Nanotechnol.* **7**, 699–712 (2012).
12. Radisavljevic, B., Radenovic, A., Brivio, J., Giacometti, V. & Kis, A. Single-layer MoS transistors. *Nat. Nanotechnol.* **6**, 147–150 (2011).
13. Bai, G. et al. 2D Layered materials of rare-earth Er-doped MoS with NIR-to-NIR down- and up-conversion photoluminescence. *Adv. Mater.* **28**, 7472–7477 (2016).
14. Jiao, L. et al. Layer-dependent photoresponse of 2D MoS films prepared by pulsed laser deposition. *J. Mater. Chem. C.* **7**, 2522–2529 (2019).
15. Yang, Z. & Hao, J. Recent progress in 2D layered III–VI semiconductors and their heterostructures for optoelectronic device applications. *Adv. Mater. Technol.* **4**, 1900108 (2019).
16. Jie, W. et al. Layer-dependent nonlinear optical properties and stability of non-centrosymmetric modification in few-layer GaSe sheets. *Angew. Chem. Int. Ed. Engl.* **54**, 1185–1189 (2015).
17. Yang, Z. et al. Wafer-scale synthesis of high-quality semiconducting two-dimensional layered InSe with broadband photoresponse. *ACS Nano* **11**, 4225–4236 (2017).
18. Anasori, B., Lukatskaya, M. R. & Gogotsi, Y. 2D metal carbides and nitrides (MXenes) for energy storage. *Nat. Rev. Mater.* **2**, 16098 (2017).
19. Pang, S. Y. et al. Universal strategy for HF-free facile and rapid synthesis of two-dimensional MXenes as multifunctional energy materials. *J. Am. Chem. Soc.* **141**, 9610–9616 (2019).
20. Liu, H., Du, Y., Deng, Y. & Ye, P. D. Semiconducting black phosphorus: synthesis, transport properties and electronic applications. *Chem. Soc. Rev.* **44**, 2732–2743 (2015).
21. Zhang, Z. et al. Manifestation of unexpected semiconducting properties in few-layer orthorhombic arsenene. *Appl. Phys. Express* **8**, 055201 (2015).
22. Zhang, S. et al. Semiconducting group 15 monolayers: a broad range of band gaps and high carrier mobilities. *Angew. Chem. Int. Ed. Engl.* **55**, 1666–1669 (2016).
23. Takao, Y., Asahina, H. & Morita, A. Electronic structure of black phosphorus in tight binding approach. *J. Phys. Soc. Jpn.* **50**, 3362–3369 (1981).
24. Tran, V., Soklaski, R., Liang, Y. & Yang, L. Layer-controlled band gap and anisotropic excitons in few-layer black phosphorus. *Phys. Rev. B* **89**, 235319 (2014).
25. Akhtar, M. et al. Recent advances in synthesis, properties, and applications of phosphorene. *npj 2D Mater. Appl.* **1**, 5 (2017).
26. Liang, L. et al. Electronic bandgap and edge reconstruction in phosphorene materials. *Nano Lett.* **14**, 6400–6406 (2014).

27. Liu, H. et al. Phosphorene: an unexplored 2D semiconductor with a high hole mobility. *ACS Nano* **8**, 4033–4041 (2014).
28. Buscema, M. et al. Fast and broadband photoresponse of few-layer black phosphorus field-effect transistors. *Nano Lett.* **14**, 3347–3352 (2014).
29. Na, J. et al. Few-layer black phosphorus field-effect transistors with reduced current fluctuation. *ACS Nano* **8**, 11753–11762 (2014).
30. Zhang, J. et al. Phosphorene nanoribbon as a promising candidate for thermoelectric applications. *Sci. Rep.* **4**, 6452 (2014).
31. Qin, G. et al. Hinge-like structure induced unusual properties of black phosphorus and new strategies to improve the thermoelectric performance. *Sci. Rep.* **4**, 6946 (2014).
32. Qiao, J., Kong, X., Hu, Z. X., Yang, F. & Ji, W. High-mobility transport anisotropy and linear dichroism in few-layer black phosphorus. *Nat. Commun.* **5**, 4475, https://doi.org/10.1038/ncomms5475 (2014).
33. Xia, F., Wang, H. & Jia, Y. Rediscovering black phosphorus as an anisotropic layered material for optoelectronics and electronics. *Nat. Commun.* **5**, 4458 (2014).
34. Fei, R. & Yang, L. Strain-engineering the anisotropic electrical conductance of few-layer black phosphorus. *Nano Lett.* **14**, 2884–2889 (2014).
35. Rodin, A. S., Carvalho, A. & Castro Neto, A. H. Strain-induced gap modification in black phosphorus. *Phys. Rev. Lett.* **112**, 176801 (2014).
36. Liu, Q., Zhang, X., Abdalla, L. B., Fazzio, A. & Zunger, A. Switching a normal insulator into a topological insulator via electric field with application to phosphorene. *Nano Lett.* **15**, 1222–1228 (2015).
37. Jiang, J. W. & Park, H. S. Negative poisson's ratio in single-layer black phosphorus. *Nat. Commun.* **5**, 4727 (2014).
38. Li, D. et al. Polarization and thickness dependent absorption properties of black phosphorus: new saturable absorber for ultrafast pulse generation. *Sci. Rep.* **5**, 15899 (2015).
39. Li, L. et al. Quantum Hall effect in black phosphorus two-dimensional electron system. *Nat. Nanotechnol.* **11**, 593–597 (2016).
40. Moreno-Moreno, M., Lopez-Polin, G., Castellanos-Gomez, A., Gomez-Navarro, C. & Gomez-Herrero, J. Environmental effects in mechanical properties of few-layer black phosphorus. *2D Mater.* **3**, 031007 (2016).
41. Pumera, M. & Sofer, Z. 2D Monoelemental arsenene, antimonene, and bismuthene: beyond black phosphorus. *Adv. Mater.* **29**, 1605299 (2017).
42. Zhang, S., Yan, Z., Li, Y., Chen, Z. & Zeng, H. Atomically thin arsenene and antimonene: semimetal-semiconductor and indirect-direct band-gap transitions. *Angew. Chem. Int. Ed. Engl.* **54**, 3112–3115 (2015).
43. Yang, Z., Wu, Z., Lyu, Y. & Hao, J. Centimeter-scale growth of two-dimensional layered high-mobility bismuth films by pulsed laser deposition. *InfoMat* **1**, 98–107 (2019).
44. Chen, P., Li, N., Chen, X., Ong, W.-J. & Zhao, X. The rising star of 2D black phosphorus beyond graphene: synthesis, properties and electronic applications. *2D Mater.* **5**, 014002 (2017).
45. Zhang, J. L. et al. Epitaxial growth of single layer blue phosphorus: a new phase of two-dimensional phosphorus. *Nano Lett.* **16**, 4903–4908 (2016).
46. Hu, Y. et al. van der Waals epitaxial growth and interfacial passivation of two-dimensional single-crystalline few-layer gray arsenic nanoflakes. *Chem. Mater.* **31**, 4524–4535 (2019).
47. Fortin-Deschênes, M. & Moutanabbir, O. Recovering the semiconductor properties of the epitaxial group V 2D materials antimonene and arsenene. *J. Phys. Chem. C.* **122**, 9162–9168 (2018).
48. Shao, Y. et al. epitaxial growth of flat antimonene monolayer: a new honeycomb analogue of graphene. *Nano Lett.* **18**, 2133–2139 (2018).
49. Wu, X. et al. Epitaxial growth and air-stability of monolayer antimonene on $PdTe_2$. *Adv. Mater.* **29**, 1605407 (2017).
50. Gusmao, R., Sofer, Z., Bousa, D. & Pumera, M. Pnictogen (As, Sb, Bi) nanosheets for electrochemical applications are produced by shear exfoliation using kitchen blenders. *Angew. Chem. Int. Ed. Engl.* **56**, 14417–14422 (2017).
51. Tsai, H.-S. et al. Direct synthesis and practical bandgap estimation of multilayer arsenene nanoribbons. *Chem. Mater.* **28**, 425–429 (2016).
52. Tsai, H. S., Chen, C. W., Hsiao, C. H., Ouyang, H. & Liang, J. H. The advent of multilayer antimonene nanoribbons with room temperature orange light emission. *Chem. Commun. (Camb.)* **52**, 8409–8412 (2016).
53. Gibaja, C. et al. Few-layer antimonene by liquid-phase exfoliation. *Angew. Chem. Int. Ed. Engl.* **55**, 14345–14349 (2016).
54. Ji, J. et al. Two-dimensional antimonene single crystals grown by van der Waals epitaxy. *Nat. Commun.* **7**, 13352 (2016).
55. Lu, L. et al. Broadband nonlinear optical response in few-layer antimonene and antimonene quantum dots: a promising optical Kerr media with enhanced stability. *Adv. Opt. Mater.* **5**, 1700301 (2017).
56. Lu, L. et al. Few-layer bismuthene: sonochemical exfoliation, nonlinear optics and applications for ultrafast photonics with enhanced stability. *Laser Photonics Rev.* **12**, 1700221 (2018).
57. Hussain, N. et al. Ultrathin Bi nanosheets with superior photoluminescence. *Small* **13**, 1701349 (2017).
58. Reis, F. et al. Bismuthene on a SiC substrate: a candidate for a high-temperature quantum spin Hall material. *Science* **357**, 287–290 (2017).
59. Gu, C. et al. Growth of quasi-free-standing single-layer blue phosphorus on tellurium monolayer functionalized Au(111). *ACS Nano* **11**, 4943–4949 (2017).
60. Xu, J.-P. et al. One-dimensional phosphorus chain and two-dimensional blue phosphorene grown on Au(111) by molecular-beam epitaxy. *Phys. Rev. Mater.* **1**, 061002 (2017).
61. Fu, B., Feng, W., Zhou, X. & Yao, Y. Effects of hole doping and strain on magnetism in buckled phosphorene and arsenene. *2D Mater.* **4**, 025107 (2017).
62. Bridgman, P. Two new modifications of phosphorus. *J. Am. Chem. Soc.* **36**, 1344–1363 (1914).
63. Li, L. et al. Black phosphorus field-effect transistors. *Nat. Nanotechnol.* **9**, 372–377 (2014).
64. Yasaei, P. et al. High-quality black phosphorus atomic layers by liquid-phase exfoliation. *Adv. Mater.* **27**, 1887–1892 (2015).
65. Ling, X., Wang, H., Huang, S., Xia, F. & Dresselhaus, M. S. The renaissance of black phosphorus. *Proc. Natl Acad. Sci. USA* **112**, 4523–4530 (2015).
66. Asahina, H., Shindo, K. & Morita, A. Electronic structure of black phosphorus in self-consistent pseudopotential approach. *J. Phys. Soc. Jpn.* **51**, 1193–1199 (1982).
67. Lu, W. et al. Plasma-assisted fabrication of monolayer phosphorene and its Raman characterization. *Nano Res* **7**, 853–859 (2014).
68. Zhang, S. et al. Extraordinary photoluminescence and strong temperature/angle-dependent Raman responses in few-layer phosphorene. *ACS Nano* **8**, 9590–9596 (2014).
69. Dong, S. et al. Ultralow-frequency collective compression mode and strong interlayer coupling in multilayer black phosphorus. *Phys. Rev. Lett.* **116**, 087401 (2016).
70. Dai, J. & Zeng, X. C. Bilayer phosphorene: effect of stacking order on bandgap and its potential applications in thin-film solar cells. *J. Phys. Chem. Lett.* **5**, 1289–1293 (2014).
71. Appalakondaiah, S., Vaitheeswaran, G., Lebègue, S., Christensen, N. E. & Svane, A. Effect of van der Waals interactions on the structural and elastic properties of black phosphorus. *Phys. Rev. B* **86**, 035105 (2012).
72. Wood, J. D. et al. Effective passivation of exfoliated black phosphorus transistors against ambient degradation. *Nano Lett.* **14**, 6964–6970 (2014).
73. Ryder, C. R. et al. Covalent functionalization and passivation of exfoliated black phosphorus via aryl diazonium chemistry. *Nat. Chem.* **8**, 597–602 (2016).
74. Yang, Z. et al. Field-effect transistors based on amorphous black phosphorus ultrathin films by pulsed laser deposition. *Adv. Mater.* **27**, 3748–3754 (2015).
75. Bellus, M. Z., Yang, Z., Hao, J., Ping Lau, S. & Zhao, H. Amorphous two-dimensional black phosphorus with exceptional photocarrier transport properties. *2D Mater.* **4**, 025063 (2017).
76. Bellus, M. Z. et al. Efficient hole transfer from monolayer WS to ultrathin amorphous black phosphorus. *Nanoscale Horiz.* **4**, 236–242 (2019).
77. Kang, J. et al. Probing out-of-plane charge transport in black phosphorus with graphene-contacted vertical field-effect transistors. *Nano Lett.* **16**, 2580–2585 (2016).
78. Wu, F. et al. High efficiency and fast van der Waals hetero-photodiodes with a unilateral depletion region. *Nat. Commun.* **10**, 4663 (2019).
79. Sofer, Z. et al. Layered black phosphorus: strongly anisotropic magnetic, electronic, and electron-transfer properties. *Angew. Chem. Int. Ed. Engl.* **55**, 3382–3386 (2016).
80. Han, X., Stewart, H. M., Shevlin, S. A., Catlow, C. R. & Guo, Z. X. Strain and orientation modulated bandgaps and effective masses of phosphorene nanoribbons. *Nano Lett.* **14**, 4607–4614 (2014).
81. Wang, X. et al. Highly anisotropic and robust excitons in monolayer black phosphorus. *Nat. Nanotechnol.* **10**, 517–521 (2015).
82. Luo, Z. et al. Anisotropic in-plane thermal conductivity observed in few-layer black phosphorus. *Nat. Commun.* **6**, 8572 (2015).
83. Jiang, J. W. Thermal conduction in single-layer black phosphorus: highly anisotropic? *Nanotechnology* **26**, 055701 (2015).
84. Cao, X. & Guo, J. Simulation of phosphorene field-effect transistor at the scaling limit. *IEEE Trans. Electron. Dev.* **62**, 659–665 (2014).
85. Fischetti, M. V., Fu, B. & Vandenberghe, W. G. Theoretical study of the gate leakage current in sub-10-nm field-effect transistors. *IEEE Trans. Electron. Dev.* **60**, 3862–3869 (2013).
86. Peng, X., Wei, Q. & Copple, A. Strain-engineered direct-indirect band gap transition and its mechanism in two-dimensional phosphorene. *Phys. Rev. B* **90**, 085402 (2014).
87. Taghizadeh Sisakht, E., Fazileh, F., Zare, M. H., Zarenia, M. & Peeters, F. M. Strain-induced topological phase transition in phosphorene and in phosphorene nanoribbons. *Phys. Rev. B* **94**, 085417 (2016).

88. Çakir, D., Sahin, H. & Peeters, F. M. Tuning of the electronic and optical properties of single-layer black phosphorus by strain. *Phys. Rev. B* **90**, 205421 (2014).
89. Peng, R. et al. Midinfrared electro-optic modulation in few-layer black phosphorus. *Nano Lett.* **17**, 6315–6320 (2017).
90. Whitney, W. S. et al. Field effect optoelectronic modulation of quantum-confined carriers in black phosphorus. *Nano Lett.* **17**, 78–84 (2017).
91. Liu, Y. et al. Gate-tunable giant stark effect in few-layer black phosphorus. *Nano Lett.* **17**, 1970–1977 (2017).
92. Sherrott, M. C. et al. Anisotropic quantum well electro-optics in few-layer black phosphorus. *Nano Lett.* **19**, 269–276 (2019).
93. Wang, Y. et al. Many-body effect, carrier mobility, and device performance of hexagonal arsenene and antimonene. *Chem. Mater.* **29**, 2191–2201 (2017).
94. Xu, J. H., Wang, E. G., Ting, C. S. & Su, W. P. Tight-binding theory of the electronic structures for rhombohedral semimetals. *Phys. Rev. B Condens. Matter* **48**, 17271–17279 (1993).
95. Krebs, H., Holz, W. & Worms, K. H. Über die Struktur und die Eigenschaften der Halbmetalle, X. Eine Neue Rhombische Arsenmodifikation und Ihre Mischkristallbildung mit Schwarzem Phosphor. *Chem. Ber.* **90**, 1031–1037 (1957).
96. Ma, S., Zhou, P., Sun, L. Z. & Zhang, K. W. Two-dimensional tricycle arsenene with a direct band gap. *Phys. Chem. Chem. Phys.* **18**, 8723–8729 (2016).
97. Xie, M. et al. A promising two-dimensional solar cell donor: black arsenic–phosphorus monolayer with 1.54 eV direct bandgap and mobility exceeding 14,000 cm V s. *Nano Energy* **28**, 433–439 (2016).
98. Yang, J. Y. & Liu, L. H. Temperature-dependent dielectric functions in atomically thin graphene, silicene, and arsenene. *Appl. Phys. Lett.* **107**, 091902 (2015).
99. Zhong, M. et al. Thickness-dependent carrier transport characteristics of a new 2D elemental semiconductor: black arsenic. *Adv. Funct. Mater.* **28**, 1802581 (2018).
100. Zhang, H., Ma, Y. & Chen, Z. Quantum spin hall insulators in strain-modified arsenene. *Nanoscale* **7**, 19152–19159 (2015).
101. Chen, Y. et al. Black arsenic: a layered semiconductor with extreme in-plane anisotropy. *Adv. Mater.* **30**, 1800754 (2018).
102. Zeraati, M., Vaez Allaei, S. M., Abdolhosseini Sarsari, I., Pourfath, M. & Donadio, D. Highly anisotropic thermal conductivity of arsenene: Anab initiostudy. *Phys. Rev. B* **93**, 085424 (2016).
103. Chaves, A., Mayers, M. Z., Peeters, F. M. & Reichman, D. R. Theoretical investigation of electron-hole complexes in anisotropic two-dimensional materials. *Phys. Rev. B* **93**, 115314 (2016).
104. Park, C.-M. et al. High-rate capability and enhanced cyclability of antimony-based composites for lithium rechargeable batteries. *J. Electrochem. Soc.* **154**, A917–A920 (2007).
105. Ares, P. et al. Mechanical isolation of highly stable antimonene under ambient conditions. *Adv. Mater.* **28**, 6332–6336 (2016).
106. Hu, Y., Wu, Y. & Zhang, S. Influences of Stone–Wales defects on the structure, stability and electronic properties of antimonene: a first principle study. *Phys. B Condens. Matter* **503**, 126–129 (2016).
107. Cheung, C. H., Fuh, H. R., Hsu, M. C., Lin, Y. C. & Chang, C. R. Spin Orbit coupling gap and indirect gap in strain-tuned topological insulator-antimonene. *Nanoscale Res. Lett.* **11**, 459 (2016).
108. Yang, L., Song, Y., Mi, W. & Wang, X. The electronic structure and spin–orbit-induced spin splitting in antimonene with vacancy defects. *RSC Adv.* **6**, 66140–66146 (2016).
109. Gupta, S. K., Sonvane, Y., Wang, G. & Pandey, R. Size and edge roughness effects on thermal conductivity of pristine antimonene allotropes. *Chem. Phys. Lett.* **641**, 169–172 (2015).
110. Singh, D., Gupta, S. K., Sonvane, Y. & Lukacevic, I. Antimonene: a monolayer material for ultraviolet optical nanodevices. *J. Mater. Chem. C.* **4**, 6386–6390 (2016).
111. Kim, S. H. et al. Topological phase transition and quantum spin Hall edge states of antimony few layers. *Sci. Rep.* **6**, 33193 (2016).
112. Lei, T. et al. Electronic structure of antimonene grown on $Sb_2Te_3$ (111) and $Bi_2Te_3$ substrates. *J. Appl. Phys.* **119**, 015302 (2016).
113. Wang, G., Pandey, R. & Karna, S. P. Atomically thin group V elemental films: theoretical investigations of antimonene allotropes. *ACS Appl. Mater. Interfaces* **7**, 11490–11496 (2015).
114. Zhao, M., Zhang, X. & Li, L. Strain-driven band inversion and topological aspects in Antimonene. *Sci. Rep.* **5**, 16108 (2015).
115. Aktürk, O. Ü., Özçelik, V. O. & Ciraci, S. Single-layer crystalline phases of antimony: antimonenes. *Phys. Rev. B* **91**, 235446 (2015).
116. Lu, Y. et al. Topological properties determined by atomic buckling in self-assembled ultrathin Bi(110). *Nano Lett.* **15**, 80–87 (2015).
117. Freitas, R. R. Q. et al. Topological insulating phases in two-dimensional bismuth-containing single layers preserved by hydrogenation. *J. Phys. Chem. C.* **119**, 23599–23606 (2015).
118. Ersan, F., Aktürk, E. & Ciraci, S. Stable single-layer structure of group-V elements. *Phys. Rev. B* **94**, 245417 (2016).
119. Aktürk, E., Aktürk, O. Ü. & Ciraci, S. Single and bilayer bismuthene: stability at high temperature and mechanical and electronic properties. *Phys. Rev. B* **94**, 014115 (2016).
120. Cheng, L. et al. Thermoelectric properties of a monolayer bismuth. *J. Phys. Chem. C.* **118**, 904–910 (2013).
121. Sun, J. T. et al. Energy-gap opening in a Bi 110 nanoribbon induced by edge reconstruction. *Phys. Rev. Lett.* **109**, 246804 (2012).
122. Du, H. et al. Surface Landau levels and spin states in bismuth (111) ultrathin films. *Nat. Commun.* **7**, 10814 (2016).
123. Takayama, A., Sato, T., Souma, S., Oguchi, T. & Takahashi, T. Tunable spin polarization in bismuth ultrathin film on Si(111). *Nano Lett.* **12**, 1776–1779 (2012).
124. Murakami, S. Quantum spin Hall effect and enhanced magnetic response by spin-orbit coupling. *Phys. Rev. Lett.* **97**, 236805 (2006).
125. Lu, L. et al. All-optical switching of two continuous waves in few layer bismuthene based on spatial cross-phase modulation. *ACS Photonics* **4**, 2852–2861 (2017).
126. Yao, J. D., Shao, J. M. & Yang, G. W. Ultra-broadband and high-responsive photodetectors based on bismuth film at room temperature. *Sci. Rep.* **5**, 12320 (2015).
127. Hoffman, C. A. et al. Semimetal-to-semiconductor transition in bismuth thin films. *Phys. Rev. B Condens. Matter* **48**, 11431–11434 (1993).
128. Yang, Z. & Hao, J. Progress in pulsed laser deposited two-dimensional layered materials for device applications. *J. Mater. Chem. C.* **4**, 8859–8878 (2016).
129. Yang, Z. & Hao, J. Recent progress in black-phosphorus-based heterostructures for device applications. *Small Methods* **2**, 1700296 (2018).
130. Yang, F. et al. Large magnetoresistance of electrodeposited single-crystal bismuth thin films. *Science* **284**, 1335–1337 (1999).
131. Zhu, Z., Collaudin, A., Fauqué, B., Kang, W. & Behnia, K. Field-induced polarization of Dirac valleys in bismuth. *Nat. Phys.* **8**, 89–94 (2011).
132. Li, L. et al. Phase transitions of Dirac electrons in bismuth. *Science* **321**, 547–550 (2008).
133. Behnia, K., Balicas, L. & Kopelevich, Y. Signatures of electron fractionalization in ultraquantum bismuth. *Science* **317**, 1729–1731 (2007).
134. Jie, W. et al. Observation of room-temperature magnetoresistance in monolayer MoS by ferromagnetic gating. *ACS Nano* **11**, 6950–6958 (2017).
135. Hirahara, T. et al. Direct observation of spin splitting in bismuth surface states. *Phys. Rev. B* **76**, 153305 (2007).
136. Koroteev, Y. M. et al. Strong spin-orbit splitting on bi surfaces. *Phys. Rev. Lett.* **93**, 046403 (2004).
137. Drozdov, I. K. et al. One-dimensional topological edge states of bismuth bilayers. *Nat. Phys.* **10**, 664–669 (2014).
138. Zhang, R. W., Zhang, C. W., Ji, W. X., Yan, S. S. & Yao, Y. G. First-principles prediction on bismuthylene monolayer as a promising quantum spin Hall insulator. *Nanoscale* **9**, 8207–8212 (2017).
139. Jie, W., Yu Hui, Y., Zhang, Y., Ping Lau, S. & Hao, J. Effects of controllable biaxial strain on the Raman spectra of monolayer graphene prepared by chemical vapor deposition. *Appl. Phys. Lett.* **102**, 223112 (2013).
140. Zhang, Y., Jie, W., Chen, P., Liu, W. & Hao, J. Ferroelectric and piezoelectric effects on the optical process in advanced materials and devices. *Adv. Mater.* **30**, 1707007 (2018).
141. Üzengi Aktürk, O., Aktürk, E. & Ciraci, S. Effects of adatoms and physisorbed molecules on the physical properties of antimonene. *Phys. Rev. B* **93**, 035450 (2016).
142. Wang, G., Pandey, R. & Karna, S. P. Effects of extrinsic point defects in phosphorene: B, C, N, O, and F adatoms. *Appl. Phys. Lett.* **106**, 173104 (2015).
143. Ersan, F., Aktürk, E. & Ciraci, S. Interaction of adatoms and molecules with single-layer arsenene phases. *J. Phys. Chem. C.* **120**, 14345–14355 (2016).
144. Ross, J. S. et al. Electrical control of neutral and charged excitons in a monolayer semiconductor. *Nat. Commun.* **4**, 1474 (2013).

## ACKNOWLEDGEMENTS

This work was supported by the National Natural Science Foundation of China (no. 51972279) and Research Grants Council (RGC) of Hong Kong (RGC GRF no. PolyU 153033/17 P and CRF no. C7036-17W).

## AUTHOR CONTRIBUTIONS

Both authors contributed equally to the literature search and writing of the manuscript.

## COMPETING INTERESTS

The authors declare no competing interests.

## ADDITIONAL INFORMATION

**Correspondence** and requests for materials should be addressed to J.H.

**Reprints and permission information** is available at http://www.nature.com/reprints

**Publisher's note** Springer Nature remains neutral with regard to jurisdictional claims in published maps and institutional affiliations.